ELSEVIER

Dynamic analysis of preload nonlinearity in a mechanical oscillator

Chengwu Duan, Rajendra Singh*

*Acoustics and Dynamics Laboratory, Department of Mechanical Engineering and The Center for Automotive Research,
The Ohio State University, Columbus, OH 43210, USA*

Abstract

New work on the dynamics of preload nonlinearity in a single degree of freedom mechanical system is described in this article. Significant computational issues that are encountered in the application of direct harmonic balance method are avoided by flipping over the force–displacement nonlinear relationship. An indirect multi-term harmonic balance method is then proposed. Unlike the traditional direct harmonic balance method, our effort is targeted toward the determination of periodic solutions of nonlinear force instead of displacement. The indirect method also allows us to evaluate the stability of periodic solutions by employing the Hill's scheme. The primary harmonic responses as exhibited by the preload nonlinearity are validated by the describing function method. Results show that, in general, the nonlinear responses depend on the value of mean load and they differ considerably from those based on linear system analysis. Primary resonance typically shows the hardening spring effect. Unstable solutions are observed in the vicinity of primary resonance as the oscillator makes a transition from a linear to a nonlinear system. Super-harmonic resonances are found under the light mean load conditions. A new instability, in the form of quasi-periodic or chaotic responses at or near the anti-resonances, is also found in our work. Finally, we successfully compare our analysis with one specific experiment that is reported in the literature.

1. Introduction

Preloaded spring elements are encountered in many practical mechanical and structural systems either due to intentional pre-compression, unintended manufacturing or heat treatment process. Fig. 1a illustrates a typical single degree of freedom (SDOF) mechanical oscillator with preload nonlinearity $\bar{f}(\bar{x})$ that is depicted in Fig. 1c. Den Hartog designated this as a system with "set-up springs with stops" [1]. Next, consider the automotive clutch (torsional system) that is shown in Fig. 1b. The engine torque is first transmitted to the friction plate through friction coupling and then it is carried over to the transmission input shaft by the flange. The coil springs are invariably designed with a certain amount of preload [2,3]. The inclusion of preload would allow the clutch to transmit higher elastic torque with the same spring deflection while providing sufficient

---

*Corresponding author. Tel.: +614 292 9044; fax: +614 292 3163.
E-mail address: singh.3@osu.edu (R. Singh).

Nomenclature

C	viscous damping coefficient
c_n	condition number for Jacobian
D	differential operator matrix
F	force
M	mass
N	number of integration points
J	Jacobian matrix
K	stiffness
R	residue vector
t	time
x	displacement
ω	excitation frequency (rad/s)
ε	perturbation
ϕ	phase angle
θ	phase
σ	conditioning factor for smoothening function
Ω	dimensionless frequency
τ	dimensionless time
ζ	damping ratio
Δ	discrete Fourier transform matrix

Subscripts

c	characteristic
L	preload
m	mean load
max	maximum

min	minimum
n	natural frequency or index
p	fluctuating component or peak

Superscripts

$-$	dimensional variable or parameter
$'$	first derivative with respect to dimensionless time
$''$	second derivative with respect to dimensionless time
-1	inverse
$+$	pseudo-inverse
T	transpose

Operators

$*$	equilibrium point
$\|\|$	absolute value
$\|\|\ \|\|$	Euclidean or L_2 norm

Abbreviations

DFM	describing function method
DFT	discrete Fourier transform
SDOF	single degree of freedom system
MHBM	multi-term harmonic balance method
max	maximum value
min	minimum value

vibration isolation. Consequently, the torque transmission capacity is increased while ensuring the reliability of the coil springs.

Literature on the preload nonlinearity is very sparse. Yoshitake and Sueoka [4] conducted bifurcation and stability analyses for such a system. However, no mean load was considered and only the direct numerical integration scheme was employed to calculate the nonlinear response. Some efforts have, however, been made to treat this problem as a piecewise linear spring by assuming a very stiff spring in the first stage. For instance, Rogers et al. [5] studied the joystick dynamics where the preload stiffness (as a stiff spring) was based on measured force–displacement profile. However, their analysis was limited to transient responses and their formulation differs considerably from the preloaded function $\bar{f}(\bar{x})$ of Fig. 1c.

Many researchers have been studied the clearance nonlinearity or piecewise linear system problems [5–10]. Babitsky has summarized the dynamics of typical systems and introduced semi-analytical approaches to such problems [6]. Recently, Kim et al. [7,8] examined multiple clearance-type nonlinearities with application to automotive transmission systems. In their study, they assumed a dual stage spring where α was the ratio between the first and second stage stiffnesses [7]. Theoretically, one could state that the same formulation with $\alpha \to \infty$ could be applied to the preload nonlinearity. However, computational issues arise due to the singularity at $\bar{x} = 0$. We will demonstrate this later in our article.
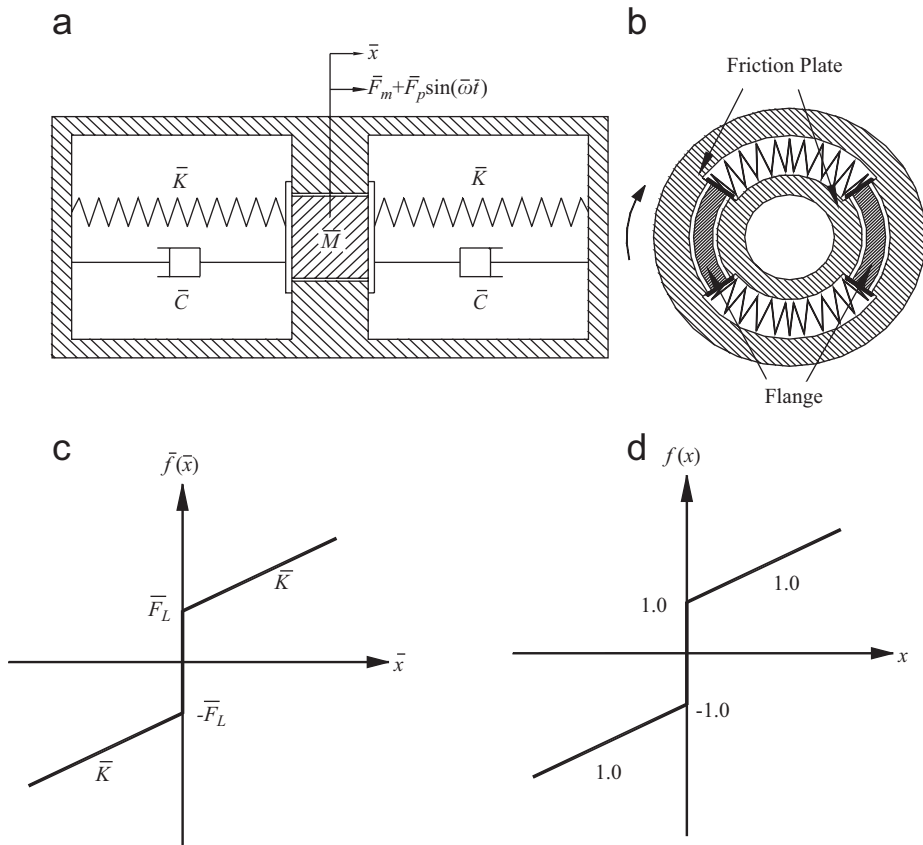
Fig. 1. Single-degree-of-freedom mechanical system with a preloaded spring $\bar{f}(\bar{x})$. (a) Schematic, similar to the one described by Den Hartog [1]. (b) Typical automotive clutch (torsional system). (c) Nonlinear force–displacement relationship with $\pm\bar{F}_L$ preload. (c) Dimensionless form with $f(x) = \pm 1.0$ preload.

2. Problem formulation

2.1. Mechanical oscillator with preload

Fig. 1a illustrates a single-degree-of-freedom translational system consisting with one mass ($\bar{M}$), two springs and two viscous dampers. The mass is under the influence of a mean load $\bar{F}_m$ and a sinusoidal force of amplitude $\bar{F}_p$ at frequency $\bar{\omega}$. The governing equation (in the dimensional form) is

$$\bar{M}\frac{\mathrm{d}^2\bar{x}}{\mathrm{d}\bar{t}^2} + \bar{C}\frac{\mathrm{d}\bar{x}}{\mathrm{d}\bar{t}} + \bar{f}(\bar{x}) = \bar{F}_m + \bar{F}_p\sin(\bar{\omega}\bar{t}), \tag{1}$$

where the dynamic displacement is $\bar{x}(\bar{t})$.

The nonlinear stiffness function $\bar{f}(\bar{x})$ of Fig. 1c can be defined in a piecewise manner as

$$\bar{f}(\bar{x}) = \begin{cases} \bar{F}_L\mathrm{sgn}(\bar{x}) + \bar{K}\bar{x}, & |\bar{x}| > 0, \\ [-\bar{F}_L \quad \bar{F}_L], & |\bar{x}| = 0, \end{cases} \tag{2}$$

where sgn is the signum function, $|\cdot|$ indicates the absolute value and $\bar{F}_L$ is the preload.

Eqs. (1) and (2) can be non-dimensionalized by introducing the following scalings:

$$\bar{\omega}_n = \sqrt{\bar{K}/\bar{M}}, \quad \zeta = \bar{C}/(2\sqrt{\bar{K}\bar{M}}), \tag{3a,b}$$

$$\bar{x}_c = \bar{F}_L / \bar{K}, \quad x = \bar{x}/\bar{x}_c, \quad F_L = \frac{\bar{F}_L}{\bar{F}_L} = 1.0, \quad F_m = \frac{\bar{F}_m}{\bar{F}_L}, \quad F_p = \frac{\bar{F}_p}{\bar{F}_L}, \tag{3c–g}$$

$$\Omega = \bar{\omega}/\bar{\omega}_n, \quad \tau = \bar{\omega}_n \bar{t}, \quad \frac{d\bar{x}}{d\bar{t}} = \bar{\omega}_n \bar{x}_c \frac{dx}{d\tau}, \quad \frac{d^2\bar{x}}{d\bar{t}^2} = \bar{\omega}_n^2 \bar{x}_c \frac{d^2 x}{d\tau^2}. \tag{3h–k}$$

Finally, we obtain the following dimensionless equation where $(.)'$ and $(.)''$ are the first and second derivatives with respect to the dimensionless time τ:

$$x'' + 2\zeta x' + f(x) = F_m + F_p \sin(\Omega\tau), \tag{4}$$

$$f(x) = \begin{cases} \operatorname{sgn}(x) + x, & |x| > 0, \\ [-1.0 \quad 1.0], & |x| = 0. \end{cases} \tag{5}$$

Refer to Fig. 1d for the dimensionless nonlinear function $f(x)$.

2.2. Objectives

The chief objective of the research described in this article is to investigate the dynamic response of Eq. (4) with the preload nonlinearity as given in Eq. (5), when excited harmonically under the influence of a mean load. An indirect multi-term harmonic balance (MHBM) is developed to overcome the computational difficulty that is typically induced by the singularity of the nonlinear force–displacement profile. Our method, for the primary harmonic response, will be validated by comparing predictions with those from the describing function method. Periodic solutions of nonlinear force and displacement are calculated and their stability evaluated. In particular, the effect of preload on the nonlinear response characteristics is studied, under both high F_m and low F_m mean loads. Finally, our analysis is compared with limited experimental work that is available in the literature.

3. Linear system analysis

As shown in Fig. 1d, if $|x|$ is positive-definite under the dynamic condition, i.e. $x(\tau) > 0$ or $x(\tau) < 0$ $\forall \tau \in [0, \infty)$, the system would strictly behave like a linear time-invariant system. Since the only difference between $x(\tau) > 0$ and $x(\tau) < 0$ is the mean operating point, we select the $x(\tau) > 0$ case for our analysis. Eq. (4) can be written in this case as

$$x'' + 2\zeta x' + 1.0 + x = F_m + F_p \sin(\Omega\tau). \tag{6}$$

The steady-state harmonic response of Eq. (6) is

$$x(\tau) = (F_m - 1.0) + \frac{F_p}{\sqrt{(1 - \Omega^2)^2 + (2\zeta\Omega)^2}} \sin(\Omega\tau - \phi), \quad \phi = \tan^{-1}\left(\frac{2\zeta\Omega}{1 - \Omega^2}\right). \tag{7a,b}$$

Since the above solution is valid only when $x(\tau) > 0$, the following criterion must be satisfied:

$$\frac{F_p}{\sqrt{(1 - \Omega^2)^2 + (2\zeta\Omega)^2}} < (F_m - 1.0). \tag{8}$$

The frequency range over which the system of Fig. 1 behaves linearly is obtained by solving the above inequality, as shown below. Here $\Omega_p = \sqrt{1 - 2\zeta^2}$ is the peak frequency of a linear SDOF system and

$$\Omega \in \left(0, \sqrt{\Omega_p^2 - \sqrt{\Omega_p^4 - \left[1 - \left(\frac{F_p}{F_m - 1.0}\right)^2\right]}}\right) \cup \left(\sqrt{\Omega_p^2 + \sqrt{\Omega_p^4 - \left[1 - \left(\frac{F_p}{F_m - 1.0}\right)^2\right]}}, \infty\right). \tag{9}$$

Further, the resulting relation also implicitly states the following condition between F_m, F_p and ζ must hold to ensure the existence of solution,

$$4\zeta^2(1 - \zeta^2) < \left(\frac{F_p}{F_m - 1.0}\right)^2. \tag{10}$$

Interestingly, the system response is always given by the linear system when the minimum response of $x(\tau)$ is higher than 0 at Ω_p. Under the following condition, the preload in the system should not affect the system dynamics except that F_L shifts the mean operating point by 1.0, thus

$$F_m - \frac{F_p}{2\zeta\sqrt{1 - \zeta^2}} > 1.0. \tag{11}$$

4. Frequency domain solution

4.1. Direct multi-term harmonic balance method

The multi-term harmonic balance method (MHBM) is a well-known technique for nonlinear system analysis, especially when periodic responses to harmonic excitation are of interest [7–10]. For example, Von Groll and Ewins [9] successfully applied the multi-term harmonic balance method to rotor/stator contact problem. Recently, Kim et al. [7] proposed a refined multi-term harmonic balance method and studied a clearance type nonlinearity with application to an automotive clutch and geared system. They conditioned the original backlash and multi-valued spring nonlinearities by defining a smoothing function along with an adjustable smoothing factor σ [10]. Further, they evaluated the effect of selecting different smoothing functions and of varying σ on the nonlinear frequency responses. Essentially, in the multi-term harmonic balance method the periodic excitation and responses are expressed as a truncated Fourier series, as shown below:

$$F(\tau) = p_0 + \sum_{n=1}^{nh} p_{2n-1} \sin(n\Omega\tau) + p_{2n} \cos(n\Omega\tau), \tag{12a}$$

$$x(\tau) = a_0 + \sum_{n=1}^{nh} a_{2n-1} \sin(n\Omega\tau) + a_{2n} \cos(n\Omega\tau), \tag{12b}$$

$$f(x) = b_0 + \sum_{n=1}^{nh} b_{2n-1} \sin(n\Omega\tau) + b_{2n} \cos(n\Omega\tau). \tag{12c}$$

Here, nh represents the number of harmonics used to construct the periodic excitation and response time histories. Noted that only the first ($nh = 1$) term of in the excitation $F(\tau)$ will be used in our study since only single frequency harmonic excitation is considered. Nonetheless, super-harmonics are included in the response series (Eqs. (12b) and (12c)). Further, we discretize the continuous $F(\tau)$ time history by N points for each period and introduce an inverse discrete Fourier transform (IDFT) matrix $\underline{\underline{\Delta}}$ and corresponding Fourier coefficients $\underline{p} = [p_0 p_1 \ldots p_{2nh}]^T$; refer to Ref. [7] for details.

$$\underline{F}(\underline{\tau}) = \begin{pmatrix} F(\tau_0) & F(\tau_1) & \cdots & F(\tau_{N-1}) \end{pmatrix}^T = \underline{\underline{\Delta}}\,\underline{p}, \tag{13a}$$

Similarly,

$$\underline{x}(\underline{\tau}) = \underline{\underline{\Delta}}\,\underline{a}, \quad \underline{f}(\underline{x}) = \underline{\underline{\Delta}}\,\underline{b}, \tag{13b,c}$$

$$\underline{\mathbf{a}} = \begin{bmatrix} a_0 & a_1 & \dots & a_{2nh} \end{bmatrix}^{\mathrm{T}}, \quad \underline{\mathbf{b}} = \begin{bmatrix} b_0 & b_1 & \dots & b_{2nh} \end{bmatrix}^{\mathrm{T}}. \tag{13d,e}$$

Introduce a differential operator $\underline{\underline{\mathbf{D}}}$ as

$$\underline{\underline{\mathbf{D}}} = \begin{bmatrix} 0 & & & & \\ & \ddots & & & \\ & & \begin{bmatrix} 0 & -n \\ n & 0 \end{bmatrix} & & \\ & & & & \ddots \end{bmatrix}. \tag{14}$$

Thus, we have:

$$\underline{\mathbf{x}}'(\underline{\tau}) = \Omega \underline{\underline{\mathbf{\Delta}}} \underline{\underline{\mathbf{D}}} \underline{\mathbf{a}}, \quad \underline{\mathbf{x}}''(\underline{\tau}) = \Omega^2 \underline{\underline{\mathbf{\Delta}}} \underline{\underline{\mathbf{D}}}^2 \underline{\mathbf{a}}. \tag{15a,b}$$

Substitute Eqs. (13–15) into Eq. (4) and define the residue $\underline{\mathbf{\Delta R}}$ in the time domain as

$$\underline{\mathbf{\Delta R}} = \Omega^2 \underline{\underline{\mathbf{\Delta}}} \underline{\underline{\mathbf{D}}}^2 \underline{\mathbf{a}} + 2\zeta\Omega \underline{\underline{\mathbf{\Delta}}} \underline{\underline{\mathbf{D}}} \underline{\mathbf{a}} + \underline{\mathbf{\Delta}} \underline{\mathbf{b}} - \underline{\mathbf{\Delta}} \underline{\mathbf{p}}. \tag{16}$$

Pre-multiply both sides by the pseudo inverse $\underline{\underline{\mathbf{\Delta}}}^{+} = (\underline{\underline{\mathbf{\Delta}}}^{\mathrm{T}} \underline{\underline{\mathbf{\Delta}}})^{-1} \underline{\underline{\mathbf{\Delta}}}^{\mathrm{T}}$, and then define the residue $\underline{\mathbf{R}}$ in harmonic domain as

$$\underline{\mathbf{R}} = \Omega^2 \underline{\underline{\mathbf{D}}}^2 \underline{\mathbf{a}} + 2\zeta\Omega \underline{\underline{\mathbf{D}}} \underline{\mathbf{a}} + \underline{\mathbf{b}} - \underline{\mathbf{p}}. \tag{17}$$

Typically, in the multi-term harmonic balance method, the displacement response is calculated directly [6,7], thus a Jacobian matrix is calculated and then $\underline{\mathbf{a}}$ is updated at each iteration step:

$$\underline{\underline{\mathbf{J}}} = \frac{\partial \underline{\mathbf{R}}}{\partial \underline{\mathbf{a}}} = (\Omega^2 \underline{\underline{\mathbf{D}}}^2 + 2\zeta\Omega \underline{\underline{\mathbf{D}}}) + \frac{\partial \underline{\mathbf{b}}}{\partial \underline{\mathbf{a}}}, \quad \nabla \underline{\mathbf{a}} = \underline{\mathbf{a}}^k - \underline{\mathbf{a}}^{k+1} = \underline{\underline{\mathbf{J}}}^{-1} \underline{\mathbf{R}}, \tag{18a,b}$$

where $\partial \underline{\mathbf{b}} / \partial \underline{\mathbf{a}}$ can be evaluated in the following manner and the superscript + indicates the pseudo-inverse.

$$\frac{\partial \underline{\mathbf{b}}}{\partial \underline{\mathbf{a}}} = \underline{\underline{\mathbf{\Delta}}}^{+} \frac{\partial \underline{\mathbf{f}}}{\partial \underline{\mathbf{x}}} \underline{\underline{\mathbf{\Delta}}}. \tag{19}$$

As noted in Fig. 1d, when $\mathbf{x} = 0$, $\partial \underline{\mathbf{f}} / \partial \underline{\mathbf{x}} \to \infty$. Thus the calculation of $\underline{\underline{\mathbf{J}}}$ would be theoretically prohibited. This problem has been addressed in previous work on clearance nonlinearities [10] by using a smoothing function. Using that approach here, the force–displacement relationship of Eq. (5) is expressed as

$$f(x) \cong \frac{2}{\pi} \arctan(\sigma x) + x, \quad \frac{\partial f}{\partial x} \cong 1 + \frac{2}{\pi} \frac{\sigma}{1 + \sigma^2 x^2}. \tag{20a,b}$$

With this manipulation, $\underline{\underline{\mathbf{J}}}$ can be mathematically defined. However, a high value of σ is still needed to accurately represent the true $f(x)$ profile. Otherwise, spurious super-harmonic peaks will appear. For example, when $\sigma = 10$ is used, a spurious super-harmonic resonance peak appears around $\Omega = 0.54$, as shown in Fig. 2a; this peak is not present when $\sigma = 50$. Note that the maximum maps constructed by picking the maximum of $x(\tau)$ at each excitation Ω are used to represent the nonlinear frequency response characteristics. We will also use the minimum maps in the subsequent sections when necessary. In fact, Kim et al. [10] also observe similar phenomena in the frequency response of a torsional system with clearance nonlinearity. The main problem in this work is introduced by the over-conditioned non-linear $f(x)$ relationship. As shown in Fig. 3, the nonlinear $f(x)$ profiles constructed at $\Omega = 0.54$ with the calculated results with $\sigma = 10$ and 50 are quite different. In the case of $\sigma = 10$, the transition is smooth like a polynomial nonlinearity when the response x approaches zero. In contrast, the system still operates
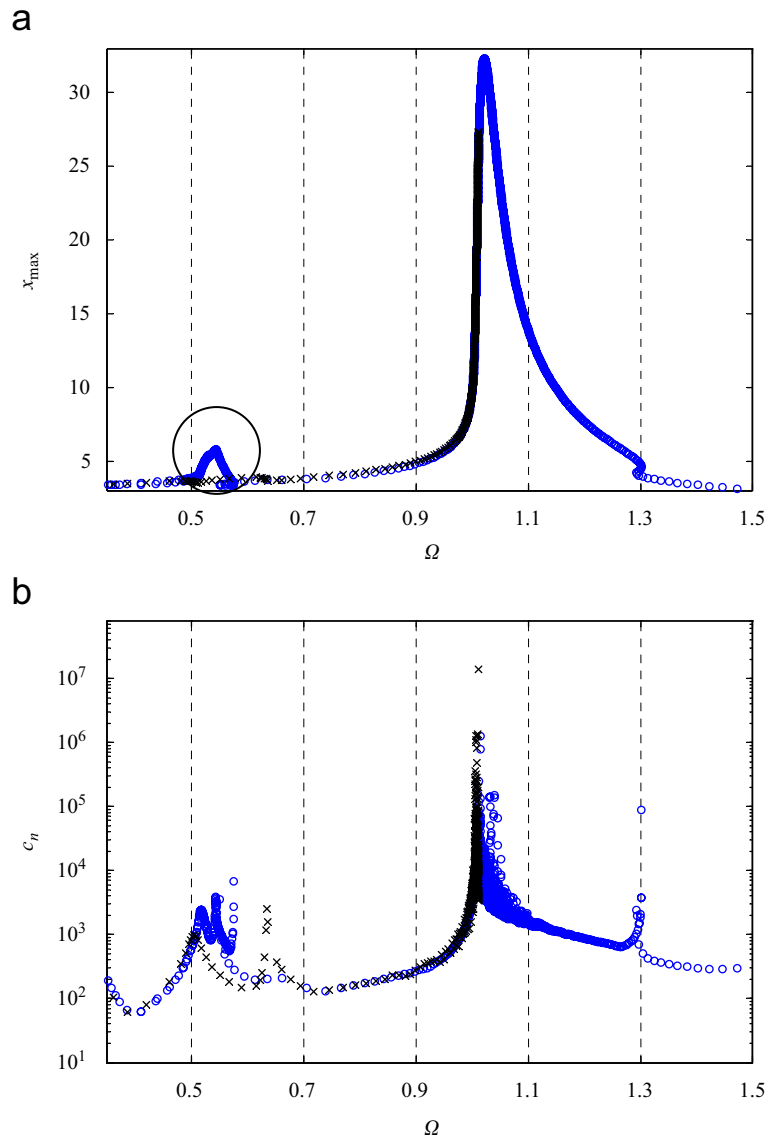
Fig. 2. Computational issues associated with direct multiple harmonic balance method given $F_m = 3.0$, $F_p = 1.2$ and $\zeta = 0.02$. (a) Effect of the smoothening factor σ and spurious super-harmonic peaks. (b) Calculated condition number of $\underline{\mathbf{J}}$. Key: 'ooo' $\sigma = 10$; 'xxx' $\sigma = 50$.

as it would with a linear spring segment when $\sigma = 50$. On the other hand, a high value of σ would significantly ill-condition $\underline{\mathbf{J}}$ and prevent convergence of the solution [10]. As shown in Fig. 2a, although $\sigma = 50$ yields a more accurate response, no convergent solutions can be found when Ω goes beyond 1.0. For the linear algebra problem, as in Eq. (18b), we can efficiently evaluate the condition of $\underline{\mathbf{J}}$ by calculating its condition number c_n [11]

$$c_n = \left\| \underline{\underline{\mathbf{J}}} \right\| \cdot \left\| \underline{\underline{\mathbf{J}}}^{-1} \right\|, \tag{21}$$

where $\|\cdot\|$ represents the L_2 norm.

The calculated condition number is plotted in Fig. 2b. As shown, when Ω approaches 1.0, c_n goes up very quickly, and when it exceeds 10^7, the computation of response cannot continue.

4.2. Indirect multi-term harmonic balance method and stability

To resolve the above-mentioned computational issues, we propose an alternative way to obtain the periodic solutions. We designate this as an indirect multi-term harmonic balance method. First, target the calculation toward the nonlinear periodic force and then retrieve the displacement, based on the definite $f(x)$ relationship. To begin with, we flip the $f(x)$ relation shown in Fig. 1d and Eq. (5) and define $x(f)$ as follows:

$$x(f) = \begin{cases} 1+f, & f < -1, \\ 0, & |f| \leqslant 1, \\ -1+f, & f > 1. \end{cases} \tag{22}$$

This relationship is illustrated in Fig. 4.
Second, use the arctangent function to smooth the non-analytical relationship:

$$x(f) \cong f + \frac{1}{2}\left\{(f-1)\mathrm{acrtan}[\sigma(f-1)] - (f+1)\mathrm{acrtan}[\sigma(f-1)]\right\}. \tag{23}$$
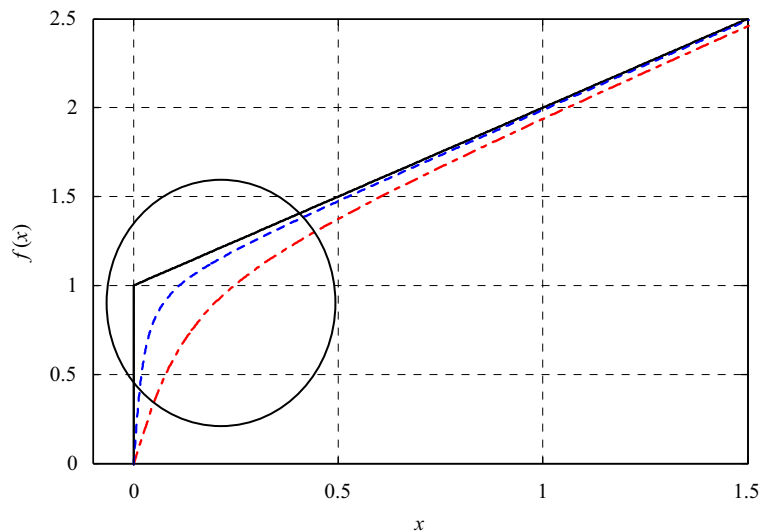

Fig. 3. Effect of the smoothening factor σ on the over-conditioned $f(x)$ profile. '—' true nonlinear profile; '-··-' conditioned $f(x)$ with $\sigma = 10$; and '---' conditioned $f(x)$ with $\sigma = 50$.
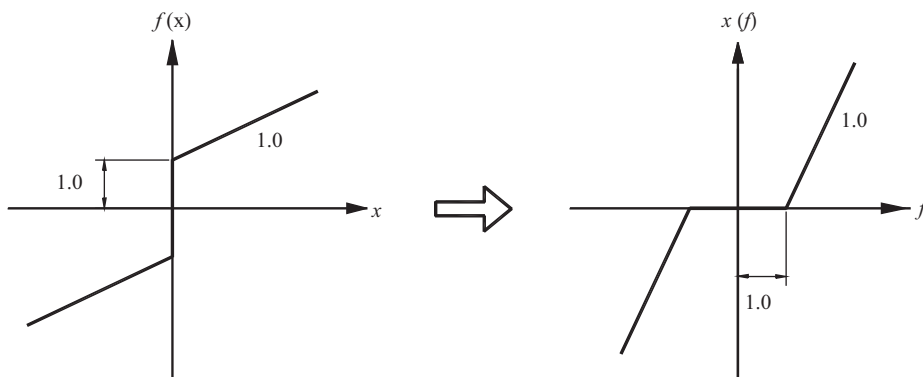

Fig. 4. Nonlinear displacement–force $f(x)$ relationship used for the Indirect Harmonic Balance Method.

Third, we reformulate the Jacobian matrix in terms of $\underline{\mathbf{b}}$ which are the harmonic coefficients of the nonlinear force:

$$\underline{\underline{\mathbf{J}}} = \frac{\partial \underline{\mathbf{R}}}{\partial \underline{\mathbf{b}}} = (\Omega^2 \underline{\underline{\mathbf{D}}}^2 + 2\zeta\Omega\,\underline{\underline{\mathbf{D}}})\frac{\partial \underline{\mathbf{a}}}{\partial \underline{\mathbf{b}}} + \underline{\underline{\mathbf{EI}}}, \tag{24}$$

where, $\underline{\underline{\mathbf{EI}}}$ is an $(2nh+1) \times (2nh+1)$ identity matrix. Fourth, $\partial\underline{\mathbf{a}}/\partial\underline{\mathbf{b}}$ is evaluated as follows:

$$\frac{\partial \underline{\mathbf{a}}}{\partial \underline{\mathbf{b}}} = \underline{\underline{\mathbf{\Delta}}}^+ \frac{\partial \underline{\mathbf{x}}}{\partial \underline{\mathbf{f}}}\underline{\underline{\mathbf{\Delta}}}. \tag{25}$$

Fifth, substitute $\underline{\underline{\mathbf{J}}}$ into the Newton–Raphson iteration and solve for $\underline{\mathbf{b}}$ or $\underline{\mathbf{f}}$. Finally, we obtain x from Eq. (23). Although Eq. (25) is just slightly different from Eq. (19), the numerical conditioning of $\underline{\underline{\mathbf{J}}}$ in Eq. (24) can be drastically improved by avoiding the essential singularity of $\partial\underline{\mathbf{f}}/\partial\underline{\mathbf{x}}$. For example, Fig. 5a presents the
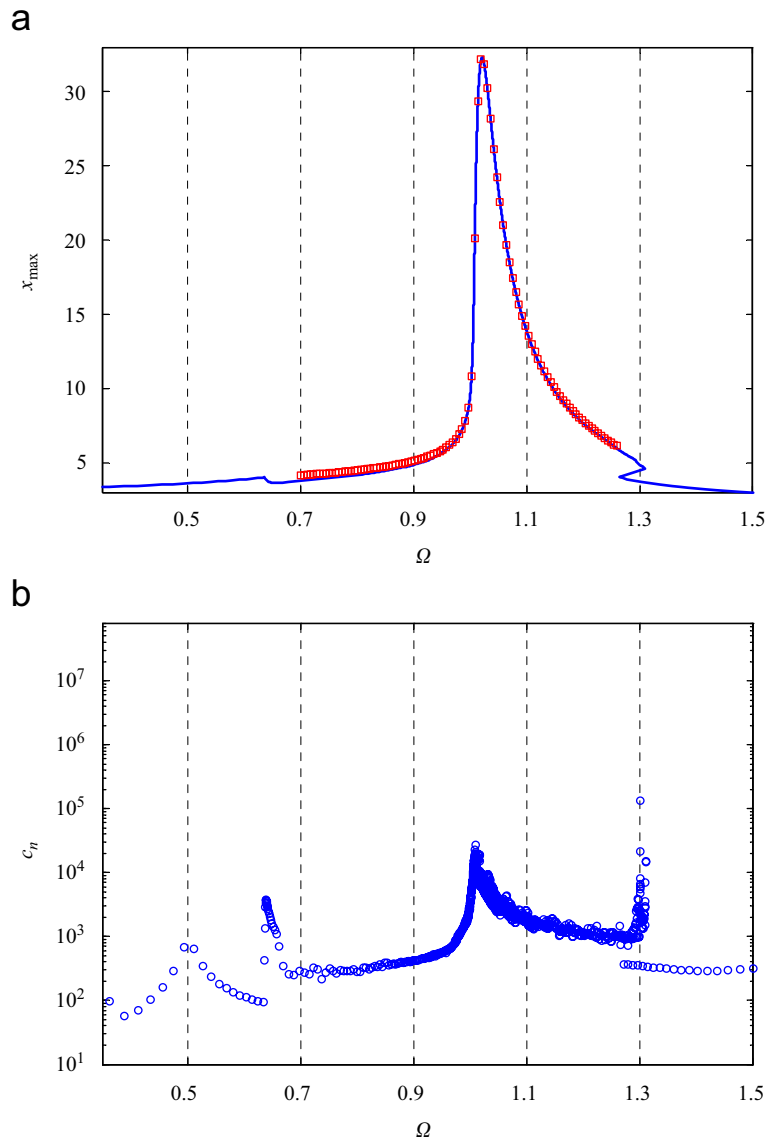

Fig. 5. Nonlinear frequency response characteristics given $F_m = 3.0$, $F_p = 1.2$ and $\zeta = 0.02$. (a) Response of x_{max}: '—' indirect MHBM solution; and 'ooo' describing function method solution. (b) Calculated condition number of $\underline{\underline{\mathbf{J}}}$.

solvability of $x_{\max}$ using the indirect HBM with $\sigma = 10^3$. As evident from Fig. 5a, the proposed indirect multi-term harmonic balance method with $\sigma = 10^3$ works well for the preload nonlinearity. Also, as illustrated in Fig. 5b, although the value of σ in the indirect multi-term harmonic balance method is much higher than in the direct method (with $\sigma = 50$), the corresponding condition number, c_n, is significantly lower.

4.3. Path following technique and stability issues

Further, the path following technique is used to calculate the turning points. The basic idea is to include $\partial \underline{R}/\partial \Omega$ as an independent variable in $\underline{J}$. Prior researchers such as Von Groll and Ewins [9] and Kim et al. [7] have clearly illustrated this. Also, we can take advantage of it in our indirect harmonic balance method without making any changes to the formulation. Prior researchers [7] have evaluated the stability of the periodic solution of $x(\tau)$. In contrast, we examine the stability of $f(\tau)$ by using Hill's method. Because $f(\tau)$ and $x(\tau)$ hold a definite relationship, they should share the same stability property. First, write $f(x, \tau)$ as $f^* + \varepsilon(\tau)$, where $f^* = f(x^*)$ is the nonlinear force at equilibrium and $\varepsilon(\tau) = s(\tau)e^{\lambda \tau}$ is the perturbation term. Here, $s(\tau)$ is a periodic time signal. Further, define $x(\tau) = x^* + \upsilon(\tau)$ where x^* is the equilibrium and $\upsilon(\tau)$ is the perturbation term. Substitute these into Eq. (4) to yield the following around the equilibrium position $x = x^*$:

$$x''|_{x=x^*} + 2\zeta x'|_{x=x^*} + f^* - (F_m + F_p(\tau)) + \upsilon''(\tau) + 2\zeta \upsilon' + \varepsilon(\tau) = 0, \tag{26}$$

or,

$$\upsilon''(\tau) + 2\zeta \upsilon' + \varepsilon(\tau) = 0. \tag{27}$$

From Eq. (23), $\upsilon' = (\partial x/\partial f)\varepsilon'$ is defined. Also, $\varepsilon' = (s' + \lambda s)e^{\lambda \tau}$ and $\varepsilon'' = (s'' + 2\lambda s' + \lambda^2 s)e^{\lambda \tau}$, thus

$$\frac{\partial x}{\partial f}(s'' + 2\lambda s' + \lambda^2 s)e^{\lambda \tau} + 2\zeta \frac{\partial x}{\partial f}(s' + \lambda s)e^{\lambda \tau} + se^{\lambda \tau} = 0. \tag{28}$$

Factor out $e^{\lambda \tau}$ and sort out the terms with the same order of λ to yield the following:

$$\left[\frac{\partial x}{\partial f}s'' + 2\zeta \frac{\partial x}{\partial f}s' + s\right] + \lambda\left[2\frac{\partial x}{\partial f}s' + 2\zeta \frac{\partial x}{\partial f}s\right] + \lambda^2\left[\frac{\partial x}{\partial f}s\right] = 0. \tag{29}$$

The periodic force $s(\tau)$ can also be discretized as $\underline{s}(\underline{\tau}) = \underline{\underline{\Delta}}\,\underline{c}$ and $\partial \underline{x}/\partial \underline{f} = \underline{\underline{\Delta}}(\partial \underline{a}/\partial \underline{b})\underline{\underline{\Delta}}^+$. Apply these in Eq. (29) and pre-multiply both sides by $\underline{\underline{\Delta}}^+$. Finally, define the following polynomial eigenvalue problem:

$$\left\{\left[\Omega^2 \frac{\partial \underline{a}}{\partial \underline{b}}\underline{\underline{D}}^2 + 2\zeta\Omega \frac{\partial \underline{a}}{\partial \underline{b}}\underline{\underline{D}} + \underline{\underline{EI}}\right] + \lambda\left[2\Omega \frac{\partial \underline{a}}{\partial \underline{b}}\underline{\underline{D}} + 2\zeta \frac{\partial \underline{a}}{\partial \underline{b}}\right] + \lambda^2\left[\frac{\partial \underline{a}}{\partial \underline{b}}\right]\right\}\underline{c} = 0, \tag{30}$$

and solve for the eigenvalues. The periodic solutions are stable if and only if all eigenvalues have negative real parts.

5. Validation of primary harmonic response using the describing function method

The describing function method is an equivalent linearization method that has been widely applied in the area of nonlinear controls [12,13]. Although it yields an approximate harmonic solution, we employ it to validate our multi-term harmonic balance analysis by comparing the solutions in the vicinity of the primary harmonic resonance. First, construct the harmonic solution in the following form:

$$x(\tau) = B + A\sin(\Omega \tau + \theta), \quad x'(\tau) = A\Omega \cos(\Omega \tau + \theta), \quad x''(\tau) = -A\Omega^2 \sin(\Omega \tau + \theta). \tag{31}$$

Since $f(x)$ is an odd function of x, the bias term B arises from F_m. With this assumption, the optimum quasi-linear approximation of $f(x)$ is expressed as [12]

$$f(\tau) = N_B B + n_p A\sin(\Omega \tau + \theta) + n_q A\cos(\Omega \tau + \theta), \tag{32}$$

$$N_B(A, B, \Omega) = \frac{1}{B}\langle f(x(0))\rangle_\theta = \frac{1}{2\pi B}\int_0^{2\pi} f(B + A\sin\theta)\,d\theta = \frac{2}{\pi B}\sin^{-1}\frac{B}{A} + 1.0, \tag{33a}$$

$$n_p(A, B, \Omega) = \frac{2}{A} \langle f(x(0)) \sin \theta \rangle_\theta = \frac{1}{\pi A} \int_0^{2\pi} f(B + A \sin \theta) \sin \theta \, d\theta = \frac{4}{\pi A} \sqrt{1 - \left(\frac{B}{A}\right)^2} + 1.0, \qquad (33b)$$

$$n_q(A, B, \Omega) = \frac{2}{A} \langle f(x(0)) \cos \theta \rangle_\theta = \frac{1}{\pi A} \int_0^{2\pi} f(B + A \sin \theta) \cos \theta \, d\theta = 0. \qquad (33c)$$

Note the above solution assumes that $A > |B|$. This also suggests the response x would actually cross the zero displacement value. Substitute Eqs. (31)–(33) into Eq. (4) and sort out the harmonic terms to obtain the following:

$$B + \frac{2}{\pi} \sin^{-1} \frac{B}{A} + \left[\frac{4}{\pi} \sqrt{1 - \frac{B^2}{A^2}} + A(1 - \Omega^2) \right] \sin(\Omega\tau + \theta) + 2\zeta A\Omega \cos(\Omega\tau + \theta) = F_m + F_p \sin(\Omega\tau), \qquad (34)$$

or,

$$B + \frac{2}{\pi} \sin^{-1} \frac{B}{A} + E \sin(\Omega\tau + \theta + \varphi) = F_m + F_p \sin(\Omega\tau). \qquad (35)$$

Further, equate the harmonic coefficients on both sides to obtain the following nonlinear algebraic equations:

$$B + \frac{2}{\pi} \sin^{-1} \frac{B}{A} = F_m, \qquad (36a)$$

$$E = \sqrt{\left[\frac{4}{\pi} \sqrt{1 - \frac{B^2}{A^2}} + A(1 - \Omega^2) \right]^2 + (2\zeta A\Omega)^2} = F_p, \qquad (36b)$$

$$\varphi = -\theta = \tan^{-1} \left(\frac{2\zeta A\Omega}{4/\pi\sqrt{1 - B^2/A^2} + A(1 - \Omega^2)} \right). \qquad (36c)$$

When only the amplitude of the response is of interest, only Eqs. (36a,b) need to be solved. Since these two equations are highly nonlinear, an explicit solution cannot be obtained unless F_m or B is zero. Instead, the Newton–Raphson scheme is used again to find the numerical solutions. Nonlinear frequency responses, as
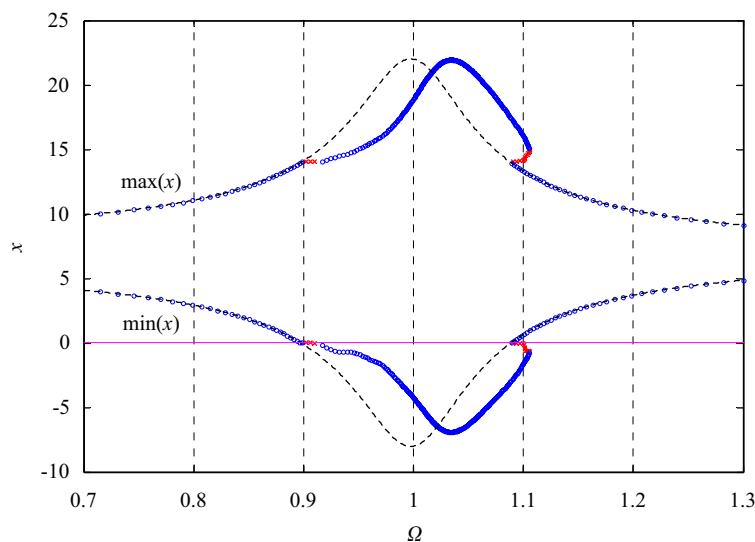

Fig. 6. Nonlinear frequency responses under heavy load: $F_m = 8.0$, $F_p = 1.5$ and $\zeta = 0.05$. '- - -' linear system analysis results; 'ooo' nonlinear stable solution; and 'xxx' nonlinear unstable solution.

predicted by the describing function method, are presented in Fig. 5a. As discussed before, the describing function method can only used in the primary harmonic regime where nonlinear behavior is followed and thus it is employed over a limited frequency range. Excellent agreement is observed between the indirect MHBM and DFM solutions in Fig. 5a. Obviously, the describing function method cannot be used to find the super-harmonic responses; that will be explored in the next section by using the indirect multi-term harmonic balance method.

6. Effect of mean load on nonlinear responses

The non-dimensionalization process described in Section 2.1 reduces the system parameters to F_m, F_p and ζ. However, our study is focused on the combined effect of excitation terms F_m and F_p and thus the damping ratio ζ is assumed to remain constant. Further, for the sake of simplicity, we would only study the effect of F_m with a given F_p. One can certainly examine other cases, such as by varying F_p with a constant F_m with the indirect multi-term harmonic balance method as proposed earlier in Section 4.2. However, it should be noted that typical nonlinear frequency response characteristics, including the crossing of zero displacements, could be demonstrated either way. In our analysis, we fix $F_p = 1.5$ and $\zeta = 0.05$, and vary F_m for the sake of illustration.
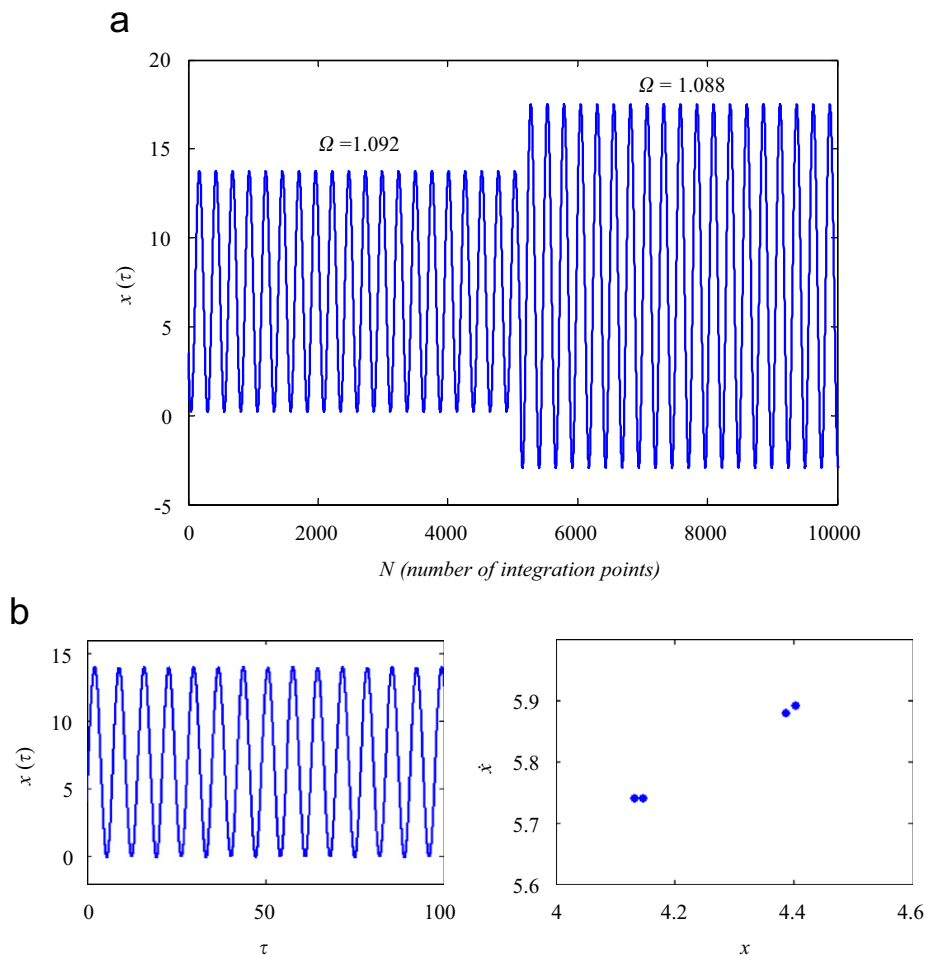

Fig. 7. Typical unstable solutions found using the numerical integration method. (a) Jump phenomenon when Ω drops from 1.092 to 1.088. (b) Time history of $x(\tau)$ and Poincare section at $\Omega = 0.9036$.

6.1. Effect of heavy mean load F_m

First, consider the case when the system operates under a heavy mean load (high F_m) condition. As shown in the linear system analysis of Section 3.1, the nonlinear response will appear only if F_m is not sufficiently larger than F_p. Given $\zeta = 0.05$ and $F_p = 1.5$, from Eq. (11) it can be seen that nonlinear analysis must be conducted when $F_m < 16$. Fig. 6 presents typical frequency responses when $F_m = 8.0$. An additional minimum curve assembling the minimum value of $x(\tau)$ at each Ω is also shown. As the frequency drops down from $\Omega = 1.3$, the locus strictly follows the linear system response and consequently a perfect overlap between the indirect multi-term harmonic balance solution and linear system analysis is obtained. However, at $\Omega \cong 1.09$, the minimum $x(\tau)$ reaches the transition point ($x = 0$, $F_L = 1.0$) and the nonlinear and linear responses separate. The linear response goes up as usual as Ω approaches 1.0. Conversely, a turning point is found in the nonlinear response. The frequency at which resonance occurs starts to increase via the automatic path following scheme. As evident from results in Fig. 6 a strong hardening spring effect is seen. This is logical since the stiffness during the preload stage (at $x = 0$) is theoretically infinite and thus the "effective spring rate" should be extremely large. For this reason, the gradient $dx/d\Omega$ approaches 0 around the turning point. Then as Ω is further increased, $\min(x)$ becomes less than 0, and the response begins to go through two transition points ($x = 0$, $F_L = 1.0$) and ($x = 0$, $F_L = -1.0$) over one period ($2\pi/\Omega$). Accordingly, the softening spring effect is observed in the response curves until it ultimately saturates at $\Omega = 1.03$. Also, unstable and multiple solutions appear around the transition point $\Omega = 1.1$. To confirm the phenomenon, a purely numerical integration solution (by using the Runge–Kutta 4th/5th order method [14]) is carried out. Jump phenomena can be clearly seen in Fig. 7a.

On the other side of primary resonance, separation between linear and nonlinear responses occurs around $\Omega \cong 0.9$ and a similar hardening spring effect immediately follows. Because the ultimate saturation phenomena including the peak frequency is always higher than 1.0, a multiple-solution regime is not observed. However, unstable solutions again appear due to the transitions that take place. Numerical integration results shown in Fig. 7b demonstrate the existence of quasi-periodic solutions, thereby confirming the semi-analytical method predictions.

6.2. Effect of light mean load F_m

Under many circumstances, mechanical systems could be operated under lighter loads (medium or low F_m). As a consequence of a relatively low value of F_m, the frequency range over which the nonlinear responses deviate from the linear system response predictions increases (see Section 3). In Fig. 8 sample results for
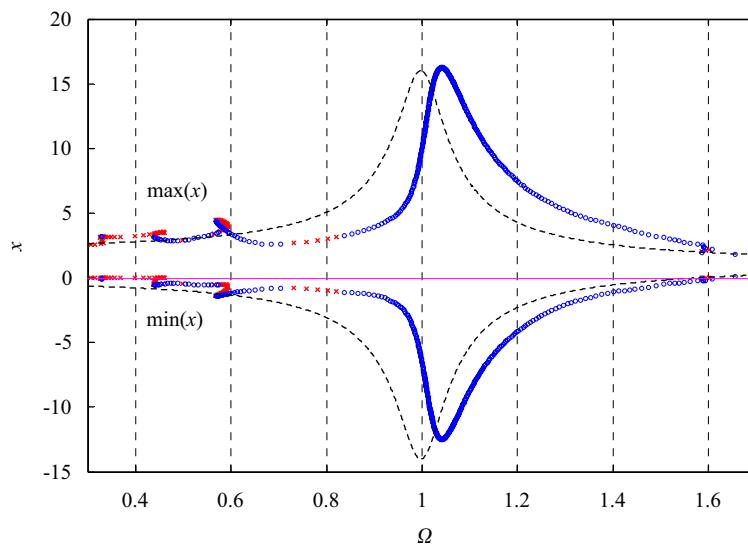

Fig. 8. Nonlinear frequency responses under a light load: $F_m = 2.0$, $F_p = 1.5$ and $\zeta = 0.05$. Key: '- - -', linear system analysis results; 'ooo' nonlinear stable solution; and 'xxx' nonlinear unstable solution.

$F_m = 2.0$ are shown. In a manner similar to the response under the heavy load operation, a transition from linear to nonlinear responses is first evident around $\Omega \cong 1.58$ Note that this is higher than the one previously discussed when $F_m = 8.0$. The similar response pattern, a hardening effect followed by saturation, is observed in the neighborhood of the primary response peak. Unlike the heavy load condition under which the responses follow the linear analysis over the lower frequency regime, the results for low F_m differ considerably from the linear system calculation. Super-harmonic resonant peaks are clearly seen around $\Omega = 0.6$ and 0.4. Although the preload nonlinearity of Fig. 1 shows an odd force–displacement relationship, both odd and even order super-harmonic resonances are excited. This phenomenon is similar to the effect of non-zero mean load that Duan and Singh found in the dry friction path study [15].

Unstable solutions occur not only in the vicinity of super-harmonic resonances but also near or at the anti-resonances. Further, unstable responses prevail up to $\Omega = 0.4$. In fact, the dynamic instability also poses significant computational problems in our multi-term harmonic balance calculations because a periodic solution is sought even when the actual solution might be unstable or aperiodic. Convergence in the numerical iteration process is hard to achieve and much time is consumed over this frequency regime. While the unstable solutions occurring at or near in the resonances can be explained by the existence of multiple equilibrium points as observed in most nonlinear systems [16], a new instability at or near the anti-resonances is revealed in our work. Indeed quasi-periodic or chaotic responses are seen in Fig. 9 where numerical time-domain results are displayed.
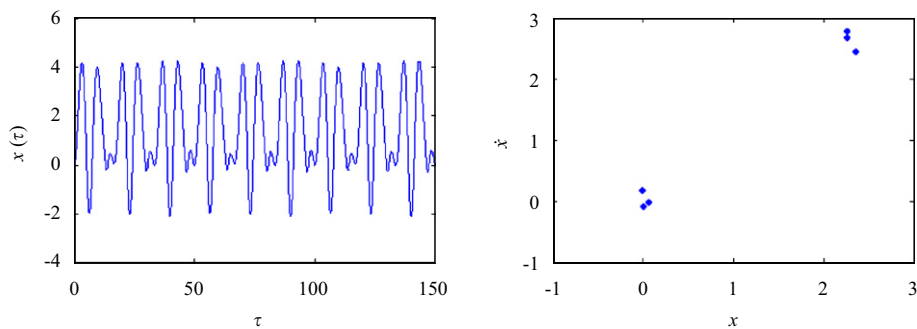

Fig. 9. Quasi-periodic solution observed at an anti-resonance: $\Omega = 0.754$, $F_m = 2.0$, $F_p = 1.5$ and $\zeta = 0.05$.
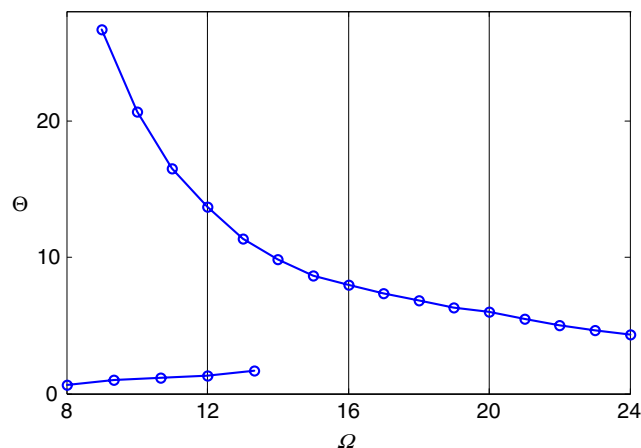

Fig. 10. Measured non-linear frequency response at resonance from the experimental results of Subach [17]. Results are re-plotted here for the sake of consistency.

7. Comparison with limited experimental results

Although the available literature on the preload nonlinearity is extremely limited, it appears that one experiment on a similar piece-wise linear system was conducted by Subach, as reported by Kononenko [17]. The measured results are shown in Fig. 10. Because we could not find the original Russian reports that are cited in Ref. [17], we cannot ascertain the exact test specifications and parameters. However, it seems that this work focused only on the resonant phenomenon and no attempts were made to find the super-harmonic peaks in his test results. Nonetheless, the trend as noted in the measured results of Fig. 10 can be compared with our analysis shown in Fig. 11. The same jump phenomenon is expected in the multiple solution regime that exhibits instability. Although the experimental results show a drastic jump down from the peak value due to a finite resolution in the excitation frequency. Our harmonic balance method analysis does not show this behavior and it can be explained by the calculated responses. At first, the response close to the peak value
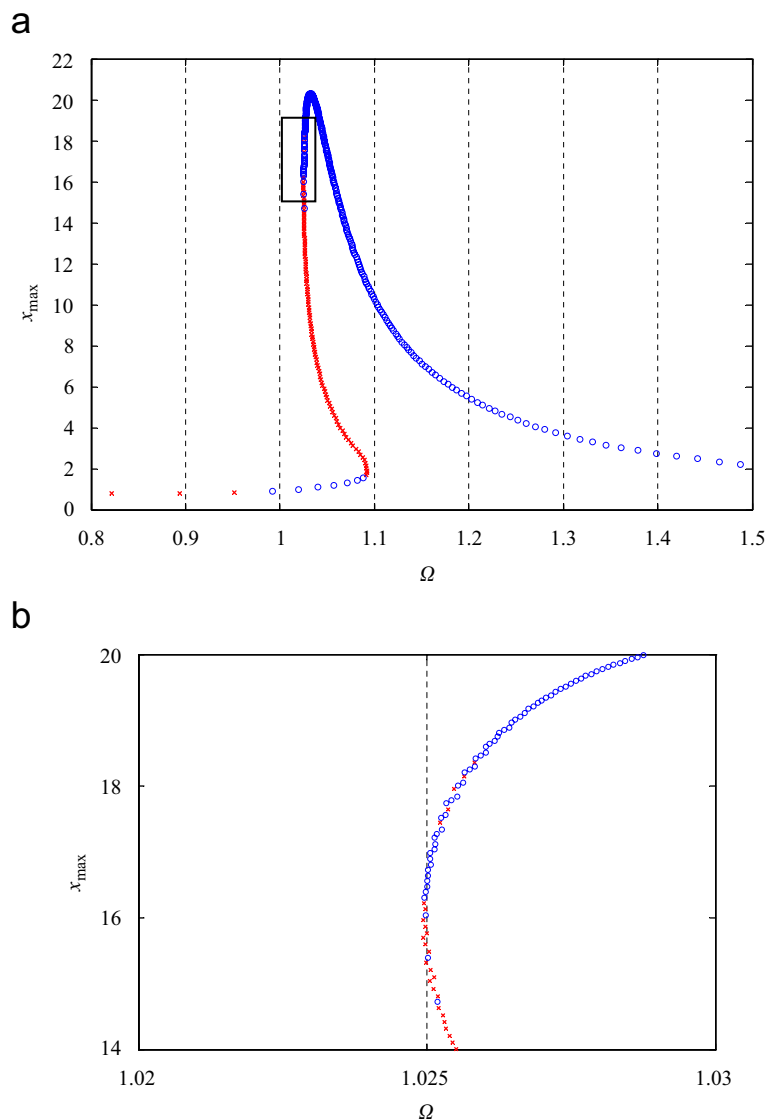

Fig. 11. Prediction yielded by the indirect multi-term harmonic balance method corresponding to the results of Fig. 10b. (a) Nonlinear frequency response. (b) Zoomed regime around the resonant peak. 'ooo' nonlinear stable solution; and 'xxx' nonlinear unstable solution.

drops very quickly though the actual values are very sensitive to a change in the excitation frequency. A coarse frequency resolution (as evident in the experimental curve) easily skips several points. Second, the dynamic responses in the vicinity of the peak are quite unstable as shown in the zoomed view of Fig. 11. This could be another reason why the experimental results just drop down directly from the peak. Overall, our analysis matches experimental results in a qualitative manner.

8. Conclusion

Dynamics of a mechanical oscillator with preload nonlinearity is introduced in this article. Two major contributions emerge. First, an indirect multi-term harmonic balance method is proposed. Unlike the traditional direct harmonic balance method, an effort is first made to determine the periodic solutions for the nonlinear force. The nonlinear displacement is then retrieved from the results for the nonlinear force given a definite force–displacement relationship. This approach permits us to overcome severe computational issues that are encountered in the direct harmonic balance method. It also allows us to evaluate the stability of periodic solutions by employing the Hill's scheme. The primary harmonic responses are validated by the describing function method. Although our method is motivated by the preload nonlinearity, we believe that it could be extended to other nonlinear systems that exhibit similar singularities. Examples include a dry friction path problem in parallel with a viscous damper and a vibro-impact system with stops. Second, nonlinear responses from those based on the system under heavy and light mean loads are studied. Results show that the nonlinear responses are quite different from the linear system analysis. Primary resonance typically occurs higher than 1.0 as a result of the hardening effect of preload nonlinearity. In the vicinity of primary resonance, unstable solutions are observed as the system makes a transition from a linear to a nonlinear system. Super-harmonic resonances are found under the light load conditions. A new instability in the form of quasi-periodic or chaotic responses at or near the anti-resonances is also found. Finally, we successfully compared our analysis with the Subach's experimental work [17] though further measurements on a preloaded system are highly desirable.

References

[1] J.P. Den Hartog, *Mechanical Vibrations*, Dover Publications, New York, 1985.
[2] Ph. Couderc, J. Callenaere, J. Der Hagopian, G. Ferraris, A. Kassai, Y. Borjesson, L. Verdillon, S. Gaimard, Vehicle driveline dynamic behaviour: experimentation and simulation, *Journal of Sound and Vibration* 218 (1998) 133–157.
[3] M.C. Tsangarides, W.E. Tobler, Dynamic behavior of a torque converter with centrifugal bypass clutch, Society of Automotive Engineering Paper 850461, 1985.
[4] Y. Yoshitake, A. Sueoka, Forced self-excited vibration with dry friction, in: M. Wiercigroch, B. de Kraker (Eds.), *Applied Nonlinear Dynamics and Chaos of Mechanical Systems with Discontinuities*, World Scientific, Singapore, 2000 (Chapter 10).
[5] R.J. Rogers, P. Garland, M. Oliver, Dynamic modelling of mechanical systems with opposing restraint preloaded stiffnesses, *Journal of Sound and Vibration* 274 (2004) 73–89.
[6] V.I. Babitsky, *Theory of Vibro-Impact Systems and Applications*, Springer, Berlin, 1998.
[7] T.C. Kim, T.E. Rook, R. Singh, Super- and sub-harmonic response calculations for a torsional system with clearance non-linearity using the harmonic balance method, *Journal of Sound and Vibration* 281 (2005) 965–993.
[8] T.C. Kim, T.E. Rook, R. Singh, Effect of non-linear impact damping on the frequency response of a torsional system with clearance, *Journal of Sound and Vibration* 281 (2004) 995–1021.
[9] G. Von Groll, D.J. Ewins, The harmonic balance method with arc-length continuation in rotor/stator contact problems, *Journal of Sound and Vibration* 241 (2001) 223–233.
[10] T.C. Kim, T.E. Rook, R. Singh, Effect of smoothening functions on the frequency response of and oscillator with clearance non-linearity, *Journal of Sound and Vibration* 263 (2003) 665–678.
[11] G. Strang, *Linear Algebra and its Applications*, Saunders College Publishing, London, 1988.
[12] A. Gelb, W.E. Vander Velde, *Multiple-Input Describing Functions and Non-linear System Design*, McGraw-Hill Book Company, New York, 1968.
[13] M. Vidyasagar, *Non-Linear Systems Analysis*, Prentice-Hall Inc., Englewood Cliffs, NJ, 1978.
[14] J.R. Dormand, P.J. Prince, A family of embedded Runge-Kutta formulae, *Journal of Computational and Applied Mathematics* 6 (1) (1980) 19–26.
[15] C. Duan, R. Singh, Super-harmonics in a torsional system with dry friction path under a mean torque, *Journal of Sound and Vibration* 285 (2005) 803–834.
[16] D.W. Jordan, P. Smith, *Non-Linear Ordinary Differential Equations*, Oxford, 1999.
[17] V.O. Kononenko, *Vibration System with a Limited Power Supply*, Iliffe Books Ltd., London, 1969.